Available online at www.sciencedirect.com

ScienceDirect

Energy Procedia 81 (2015) 1013 – 1029

Energy Procedia

69th Conference of the Italian Thermal Machines Engineering Association, ATI2014

Formula-SAE Racing Car: Experimental and Numerical Analysis of the External Aerodynamics.

Francesco Mariani[(a)*], Claudio Poggiani[(a)], Francesco Risi[(a)], Lorenzo Scappaticci[(b)]

[a]*University of Perugia, Dpt. of Industrial Engineering Via G. Duranti 67 – 06125, Perugia, Italy*
[b]*Guglielmo Marconi University, Via Plinio 44 - 00193, Rome, Italy*

Abstract

The present work aims to improve the external fluid-dynamics of the first prototype of the Formula-SAE *(Society of Automotive Engineers)* race car of the University of Perugia. In the first phase, the study concentrates its attention on the nose of the prototype; the latter has been tested in the wind tunnel of the Department of Industrial Engineering of the University of Perugia and the acquired experimental data have been used to calibrate the models used in the CFD/3D analysis.
At the same time, with the goal of decreasing the vehicle's resistance and to increase its down-force, a comparative numerical analysis was performed. The results obtained by the simulation of the complete original prototype (model *A*), are compared with those obtained from the model *B,* obtained redesigning some particulars of the model *A* or adding some appropriate aerodynamic elements such as: front wing, headrest, rear engine hood and aerodynamic extractor. The presented results show a remarkable improvement of the parameters above mentioned.
For clarity, the model A is the one that participated at the international competition of Varano (*Parma- Italy*), 2013.

Peer-review under responsibility of the Scientific Committee of ATI 2014

Keywords: wind tunnel; *CFD*; drag force; lift force; formula SAE; racing car.

Nomenclature

b. l.	boundary layers
C_D	aerodynamic drag coefficient
C_L	aerodynamic lift coefficient

*Corresponding Author. Tel: +39-075-5853732
Email address: francesco.mariani@unipg.it

Peer-review under responsibility of the Scientific Committee of ATI 2014
doi:10.1016/j.egypro.2015.12.111

CV	control volume
CFD	Computational Fluid Dynamics
D_R	aerodynamic drag [N]
S	Vehicle Frontal Area [m2]
SST	Shear Stress Transport
u	turbulent velocity distribution [m/s]
V	wind/vehicle speed [m/s]
u^*	friction velocity [m/s]
y	the normal distance from the wall to the wall-cell centroid [m]
y+	non-dimensional wall coordinate, defined as: $\boldsymbol{y \cdot u^* / \nu}$
β	dimensionless constant
ν	kinematic viscosity [m2/s]
ρ_a	air density [kg/m3]

1. Introduction

Formula SAE is a collegiate design competition where groups of students design, build and race their own open wheel race cars. Since its beginnings in the USA in 1981 [1], this formula has spread to Europe, Asia, South America and Australia, with several hundred international teams racing every year in a number of competitions held world-wide. Unlike a conventional motorsport race, teams are awarded points for eight different events, and the team with the highest cumulative total wins. There are three 'static events' (Cost, Presentation, Design) where teams are judged on their design justification, presentation and costing skills, and five 'dynamic events' (Acceleration, Skid Pan, Autocross, Fuel Economy, Endurance), which test the performance of the car and student drivers on-track [2, 3, 4, 5]. This weighted points system dictates a careful balancing of all aspects of the car design process and development. Figure 1a and 1b are the result of this process; it represents the car that attended its first competition at Varano's meeting, in September 2013.

a b

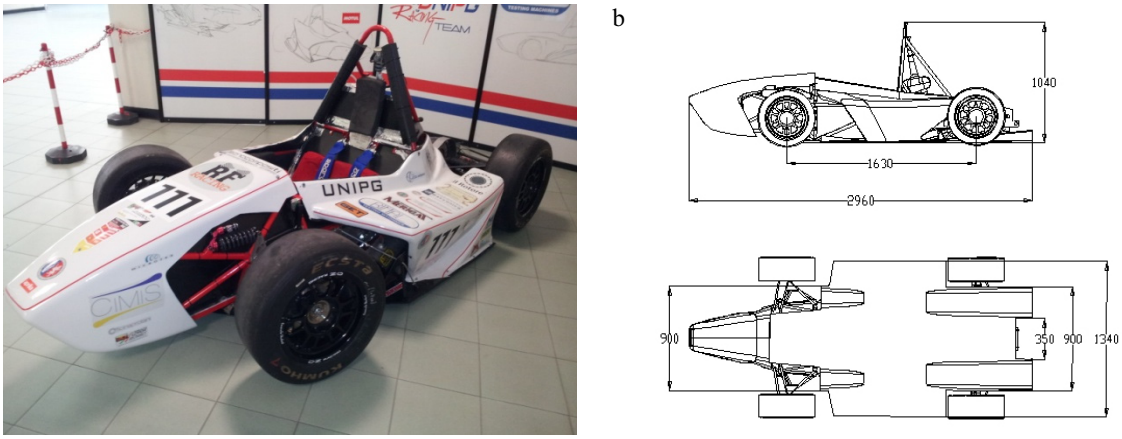

Fig. 1. (a) Formula SAE racing car; (b) Characteristics measures of the car (all dimensions are in mm).

Predicting the aerodynamics flow around industrial and racing cars, using the CFD codes, is becoming increasingly common both in the research centers and in the car companies [6, 7, 8, 9, 10, 11, 12]. This rise in interest is due to the increasing predictive capabilities of codes together with an ever more interesting reduction in the costs of computing technology. As a consequence, these tools are viable alternatives to the increasingly expensive experimental investigations.

The reduction of the aerodynamic resistance of a sports car is an achievable goal in view of the performance optimization. If one considers that the power required to overcome aerodynamic drag varies with the cube of the speed, it is understandable that even small improvements of the coefficient of aerodynamic penetration, may result in a considerable saving of the available power to the drive unit. In the specific case, the resulting decrease in fuel consumption, is surely a remarkable goal to be pursued to overcome the endurance phase: one of the five dynamic events required by the formula-SAE [6]. The ability to predict a value of the C_D as close as possible to the vehicle's operating conditions allows one to have very useful information, especially in its design stage. It is easy to imagine that, in this context, predictive tools such as the CFD codes could offer valuable assistance. In fact, the possibility of having numerical estimates very close to the experimental ones, is a considerable advantage with regard to the experimental activity executed in the wind tunnel on the prototype, being able to decrease time and development costs. An aerodynamic optimization of a vehicle can be performed both in the wind tunnel and using CFD codes; if it is a production vehicle purchased from a dealer and then transformed into a competition vehicle, the choice of the wind tunnel is practically obliged, like in [13, 14]. In fact, if one wanted to use a CFD code, one would need to perform a reverse engineering of the vehicle in order to obtain its numerical model. An aerodynamic development is presented in [15] where the authors focused attention on the shape optimization of a vehicle exposed to constant cross wind. In this case the study was carried out in wind tunnel. In [16] the authors suggest some good solutions for improving drag coefficient; even in this case, the study was conducted entirely in a wind tunnel. If instead one is the designer or somehow a member of the development team of the vehicle, the opportunity to trim the project with CFD analysis should undoubtedly be exploited [17, 18, 19].

In any case, in the first phase of the project, an experimental verification in the wind tunnel for the analysis of the correlation with numerical models, is an essential activity to develop a good aerodynamic design [20]. This even considering the fact that the modeling results, are too "mesh dependent" in order to be trusted a priori. Furthermore, the synergy between the two approaches becomes useful also in relation to the analysis of sensitivity of the models and to the optimization of the computational resources. In [21] the authors investigated the flow around a generic Sport Utility Vehicle (SUV) with two different CFD methods and compared the results with experimental data, such as aerodynamic coefficients and Particle Image Velocimetry (PIV). Results of the numerical simulations were within 3 - 7% of the measured values. In [22] the author compared the results of CFD simulations of the flow around the Ahmed body for two slant angles finding a 3% discrepancy with the experimental data.

In general, the strengths of the present work consist in having put together experimental and numerical activities applied to a real car on which, using a comparative methodology, it was possible to evaluate the aerodynamics contributions on the model coming from some changes executed on pre-existent elements and from the effects produced by the insertion of new parts.

In particular, the study is divided in two parts: the first, limited to the nose of the car, includes both experimental measurements and numerical simulations. This phase was essential both for a proper choice and tuning of the models and an in-depth mesh analysis in order to obtain an appropriate development of the boundary layer. As known, this evaluation is strictly correlated to the quality of the mesh close to the skin of the model. The main goal of this first part of the work, was to obtain a good agreement between the experimental and calculated values of the drag. This objective involves a very refined boundary layer and consequently, a large number of volumetric cells, which, in turn, imply a very high simulation time. In the present work the nose model has been discretized with 13 million volumetric cells and simulated in 46 hours, using 24 parallel processors.

The second phase, which was only numerical, compares two entire race car models named RB11.1_A and RB11.1_B respectively; that differ from each other for some changes and for some additional elements. The changes between the two models aim at decreasing the drag coefficient and to increase the down-forces trying to eliminate, at the same time, any points of recirculation and stagnation. Without affecting the physical consistency of the result, to obtain an acceptable simulation time, the total number of cells was limited considerably; reducing particularly the refining of the wall mesh.

The experimental apparatus, described in the next section, is the wind tunnel plant available to the Faculty of Engineering of the University of Perugia. The code used for the numerical activities is CCM+ (V-8.04), of ©CD-adapco.

The main characteristics of the car, including also the constraints imposed by the international federation, are summarized in Table 1.

Table 1. Formula-SAE car characteristics and regulatory constraints.

car weight	240 kg
V engine (77°) – Aprilia (sxv)	550 cm3 - 4T, 4V
bore x stroke	80x55 mm
compression ratio	12.5
max torque at 10900 RPM	65.9 N.m
max power at 13000 RPM	52 kW
intake maximum size (diameter)	20 mm
maximum allowed velocity	27.78 m/s
gear shift	5 speed
body	carbon-fiber
cooling system	liquid

2. Wind tunnel description and experimental setup

2.1 The wind tunnel of the University of Perugia

The facilities at the University of Perugia also include a Wind Tunnel in closed loop configuration (Figure 2, Figure 3a and 3b). An impeller with 11 blades in carbon warped shell, can accelerate the air to a maximum speed of 200 km/h. In each curve there are fixed blades to enhance the air flow pattern. The impeller is driven by a 375 kW electric motor. Just prior to the test room (approximately 4 m2 of effective section), the turbulence of the flow is conditioned and reduced by means of a honeycomb structure.

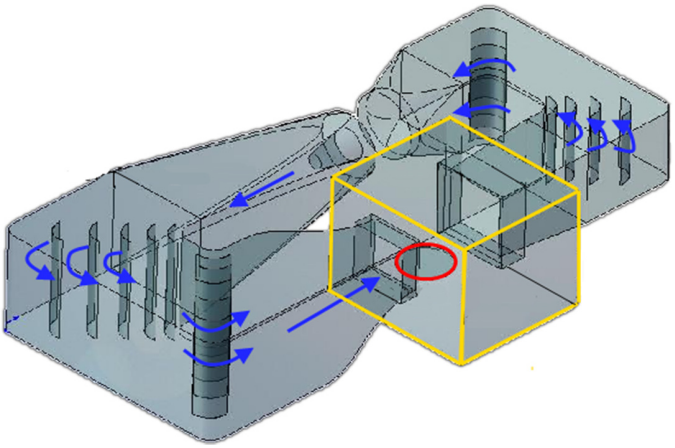

Fig. 2. Perugia Wind Tunnel facility.

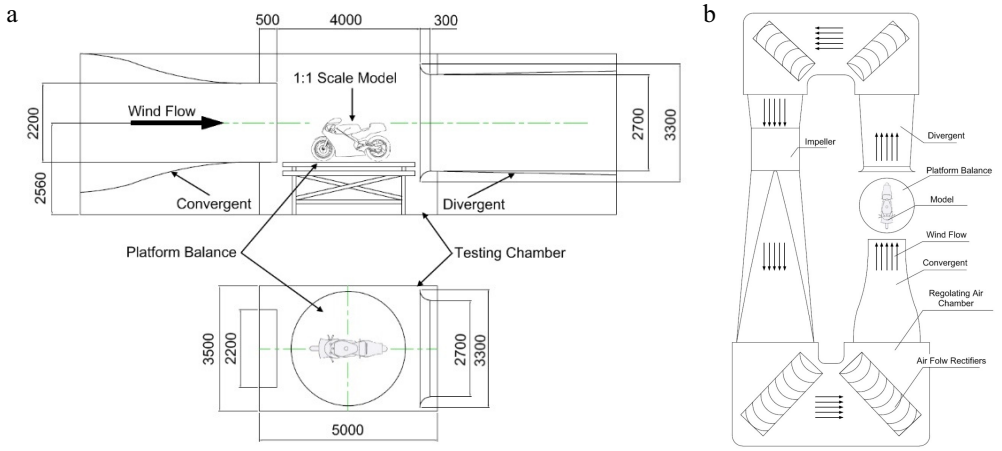

Fig. 3. (a) Wind Tunnel front view (all dimensions are in mm); (b) Wind Tunnel top view.

The flow is further accelerated by a converging duct into the testing room. Both the static and dynamic air conditions are monitored and correlated with the aerodynamic forces; two Pitot tubes monitor air speed that runs over the tested body, while a control station positioned in the testing room provides data about static air pressure, temperature and relative humidity. Aerodynamic forces are acquired by four biaxial load cells, mounted under the frame that supports the vehicle. The supporting frame is structured on three levels: the base, fixed to the ground, the top plate and the triangular structure that transfers forces. The top plate simulates the effect of the ground's aerodynamics. The signals are acquired by National Instruments cards, while the post processing is performed by a software developed by the authors in ©LabView environment, evaluating, for each of the tested configurations, the $C_D \cdot S$ value as a function of ρ_a, D_R and V collected data.

The aerodynamic drag of a vehicle linearly depends on both its characteristics of shape and frontal section S, according to the following equation:

$$C_D \cdot S = \frac{2 \cdot D_R}{\rho \cdot V^2} \tag{1}$$

where D_R is the drag resistance [N], ρ is the air density [kg/m3] and V is the vehicle/wind speed [m/s].

The total drag coefficient C_D , of a sport car is determined by a multitude of parameters. Body drag (fore-body drag, underbody drag, after-body drag, skin friction drag), internal drag (engine cooling systems), protuberance drag (wheels drag, mirrors drag, suspension parts drag, etc.), and frontal area, affect the drag resistance. All the variables mentioned above have a strong non-linear mutual influence. In general, since the aerodynamic drag is what is meant to be minimized, the drag reduction can be carried out minimizing the product $C_D \cdot S$.

2.2 Experimental setup and results

The vehicle nose used in this work was a full scale model (Figure 4a and 4b). The body was placed on the aerodynamic scales respecting both its orientation and the height from the ground, which are scheduled on the vehicle in running order. The wind tunnel test runs took about 75 seconds each, which included start up, data collection, and ramp down (Figure 5). The test were divided into three steps:

- rising speed ramp (15 s);
- regime (50 s);
- decreasing speed ramp (10 s).

Most of the tests were carried out at a regime speed value of 85 km/h for each examined configuration, repeating the run at least two times. All quantities were acquired at a 1 kHz sampling rate, while the presented data (Figure 5) were obtained by re-sampling them at 1 Hz. Tests of intuitive aerodynamic were also conducted through the use of wool tufts (Figure 4). Five runs were carried out in order to characterize the FSAE nose, in the reference condition, obtaining an averaged value of aerodynamic drag of 3,402 kg (with a standard deviation evaluated on the five samples of 0,02 kg) and a C_D*S averaged value of 0,106 (with a standard deviation of 0.001 evaluated on the five samples).

Recent experimental studies, by the same group, has been developed on different motorcycles to evaluate the influence of the speed on the aerodynamic drag. Five different full scale road motorcycles were tested in the same wind tunnel, focusing on the transient phase of rising wind speed [23].

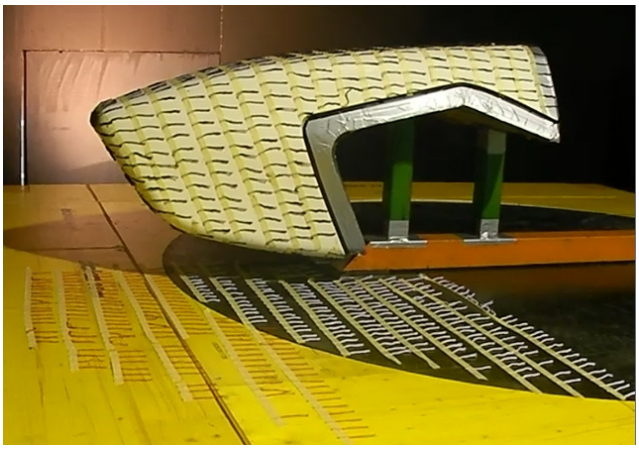

Fig. 4. (a) The vehicle's nose

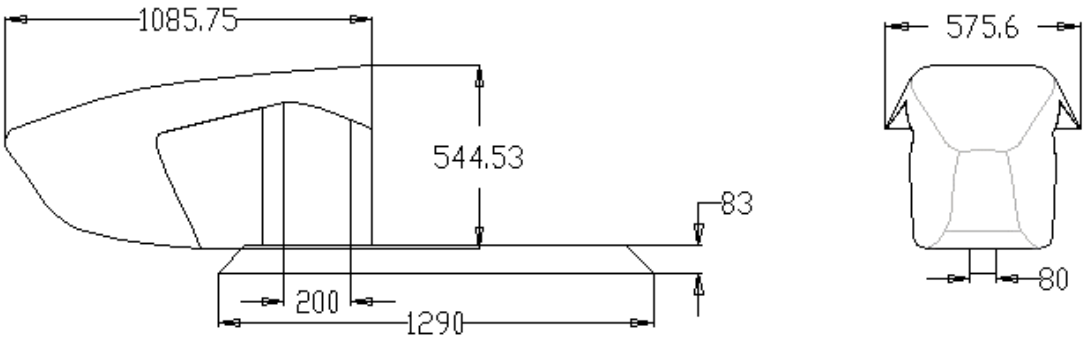

Fig. 4. (b) Characteristics measures of the nose (all dimensions are in mm).

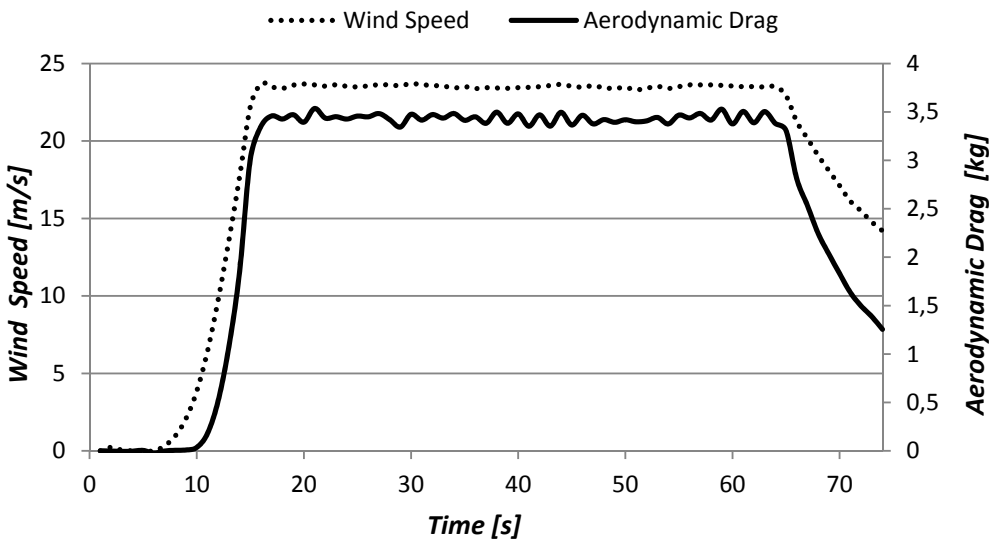

Fig. 5. Time histories of physical quantities monitored during a typical test in the wind tunnel.

3. The numerical setup

As discussed above, the present work concentrates on the measurement and on the numerical evaluation of the *drag coefficient* (C_D). In particular, the activity is divided into two main parts, the first of which concerns the experimental and numerical evaluation of the C_D. The availability of the experimental C_D value allowed the optimization of the mesh and a suitable choice of the CFD/3D models adopted. The second part follows a numerical-only approach and compares the results obtained from the simulation of the original car's geometry, with those from the simulation executed on the same car modified with some performance features. The basic terms of comparison between the two simulated models were the C_D values and the consequent down-forces.

All the simulations are configured in steady state and with the incompressible model on. As proved by a great amount of specialized literature [24, 25, 26], between the different tested models, the *k-ω SST* resulted in the best one capturing the complex turbulent phenomena in terms of displacement from the experimental evidences.

The *k-ω* model [24, 25], is one of the most used turbulence models. It is a two equation model, it includes two extra transport equations that represent the turbulent properties of the flow. The two equations take into account both the effect of the convection and the effect of the diffusion, associated to the turbulent energy. The first transported variable is the turbulent kinetic energy, *k,* while the second one is the specific dissipation, *ω*. While *ω* determines the scale of the turbulence, the first variable, *k*, determines the energy in the turbulence. The *shear stress transport* (*SST*) formulation combines the better of the two previous variables. The use of a *k-ω* formulation in the inner parts of the boundary layer makes the model directly usable all the way down to the wall through the viscous sub-layer, hence it can be used as a Low-Re turbulence model without adding any extra damping functions. This approach effectively blends a *K-Epsilon* model in the far-field with a *K-Omega* model near the wall. Finally the SST k-ω model is often appreciated for its good behavior when you are both in adverse pressure gradients and in separating flow conditions; a very common situation during the analysis of an external aero problem.

Table 2 shows the type and the values of the boundary conditions, in harmony with the experimental activity. The *control volume* (*CV*), in which is contained the model to simulate, has the same dimensions of the test chamber indicated in the previous experimental descriptions.

Table 2. Boundary type and conditions.

inlet boundary type	velocity
outlet boundary type	relative static pressure
inlet velocity value	23.5 m/s
relative static pressure value	0 Pa
test temperature	300 K

3.1. Boundary layer and mesh definition

In order to perform external aerodynamic analysis on a vehicle, three conditions must be met: the volume must be sealed, no internal geometry must be present and no overlapping or intersecting surfaces should be present. These iterative activities, together with a suitable volume mesh definition, are very time consuming steps. Concerning the mesh definition, the main attention was focused on the boundary layer (b. l.) definition; in particular, on the adoption of a suitable b. l. thickness, number of sub-layers and growing-law of the sub-layers, starting from the skin of the shell.

The dimensionless, logarithmic, universal velocity distribution law (eq. 2), for turbulent flows, asserts that the velocity, referred to the friction velocity u^*, is a function of the *dimensionless wall distance* $\boldsymbol{y}^+$:

$$\frac{u}{u*} = \frac{1}{k}[\ln(y^+) - \ln(\beta)] \tag{2}$$

The term y^+ is used as the index of the quality of the mesh near the walls and its formal definition is:

$$y^+ = \frac{y \cdot u*}{\nu} \tag{3}$$

where y is the normal distance from the wall to the wall-cell centroid, $u*$ is the friction velocity and ν is the kinematic viscosity. In problems of external flows, such as the one presented here, the best practices employed for the wall treatment, suggest for y^+ a value less or equal to 1. As shown in Figure 6, this choice has been implemented and reached in almost all the model.

For a full boundary layer development, an accurate wall treatment was adopted using a boundary layer with a thickness equal to 10mm, subdivided into 60 sub-layers, distributed starting from the shell, with a geometric progression with a *common ratio* 1.05. With these characteristics, the resulting dimension of the wall-layer is equal to $2.73 * 10^{-5}$m. Figure 7 shows the model and its *control volume*, discretized with a polyhedral mesh. Exploiting the condition of symmetry of the model the number of volumetric cells resulted of about 12 million; at the right top corner of the figure 4 it is shown a zoom of the mesh near the wall; the mesh is obtained using the *CCM+ Advanced Layer Mesh* model. This very specialized mesher allows a gradual transition from the boundary layer zone to the core of the main flux. As shown in Figure 8, this wall treatment allowed a complete development of the boundary layer. For a better readability, Figure 9 replicates with a zoom a part of the red window evidenced in Figure 8. Table 3 summarizes the main characteristics of the mesh previously described.

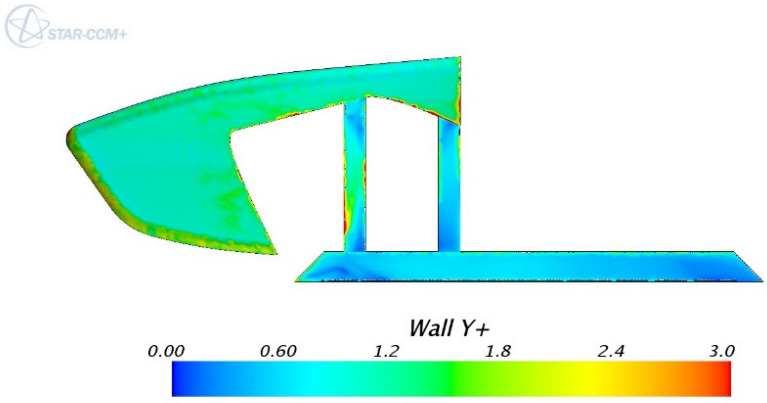

Fig. 6. Dimensionless distance (y+) on the model profile.

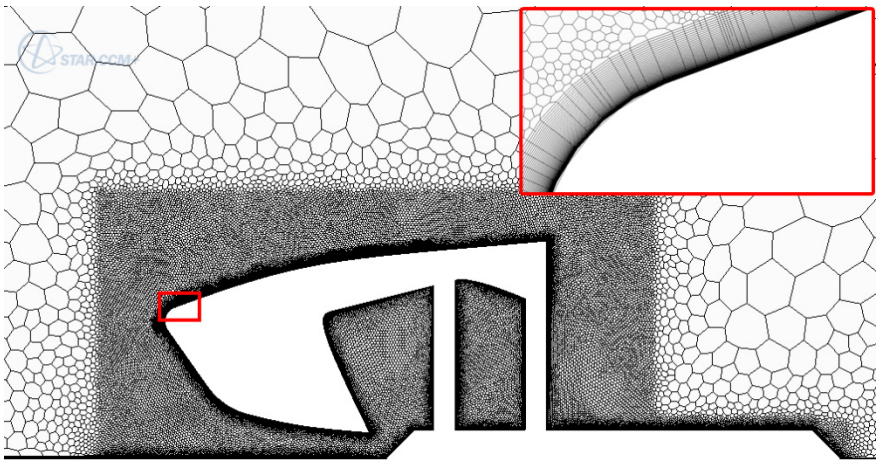

Fig. 7. Zooming of the mesh in the boundary layer.

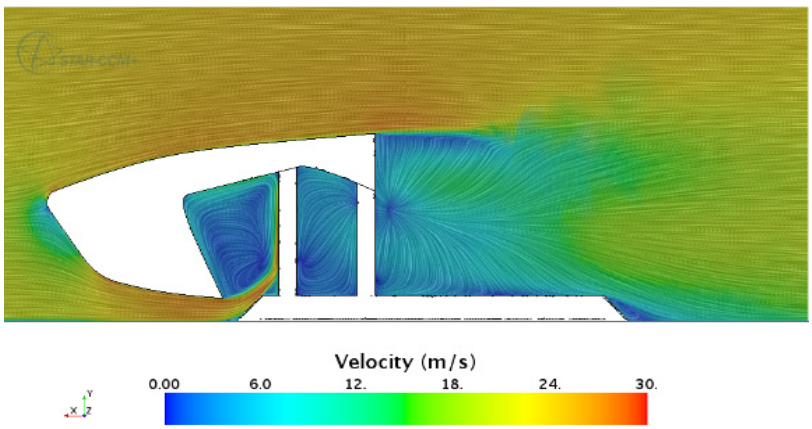

Fig. 8. Scalar velocity field on the nose.

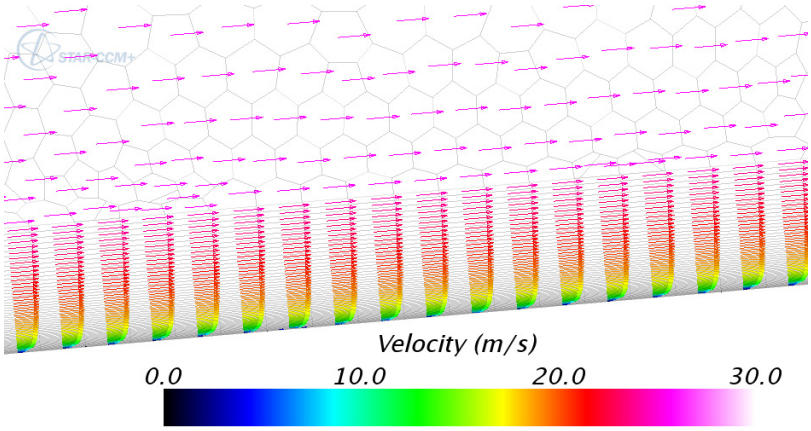

Fig. 9. Zooming of the mesh boundary layer.

Table 3. Mesh features

general mesh type	polyhedral
boundary layer mesh type	advanced layer mesh
volumetric cells	12 million
boundary layer thickness	10mm
number of sub-layers	60
geometric progression common ratio	1.05
wall-layer thickness	2.73×10^{-5} m

4. Code validation: experimental *vs* numerical results.

Some works of external aerodynamics were developed putting in synergy the experimental and numerical approaches [15, 18, 21, 27, 28]; one of the shared aim is the code validation, passing through a preliminary analysis of the mesh as one of the more important setup activities to ensure the numerical success. Both, the mesh development and the optimal model's setup are highly interdependent tasks that are decisive in determining the results of a CFD/3D simulation. To this end, the measured *drag coefficient* (C_D), was used as the global comparative parameter. As reported in the previous paragraph 2.2, this coefficient resulted equal to 0.43 against a value of 0.46, obtained from the simulation, with a consequent error equal to 6%.

Incidentally, it should be noted that the prototype, used for the experimental activity, is made of polished wood. This choice was for two reasons: the first is trivial and is related to the unavailability of the original model, transported to another location, for assembly reasons, the second for reasons of structural strength and fixing of the model to the wind-tunnel platform.

Figure 10 shows a zoom evidencing the velocity field around the stagnation point of the model.

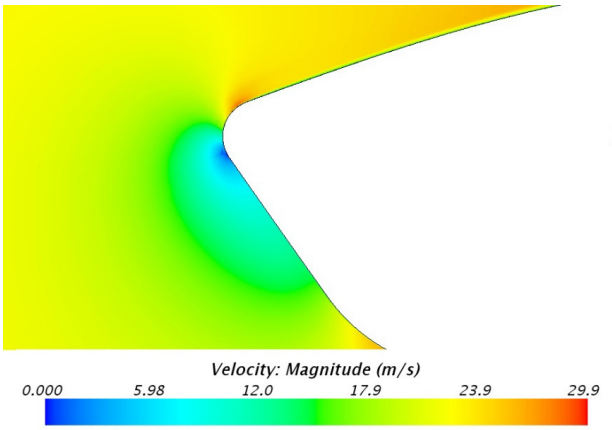

Fig. 10. Zooming the nose scalar velocity field.

5. CFD Analysis: *RB11.1_A* versus *RB11.1_B* model

5.1. General characteristics

The model *RB11.1_A* (henceforth named *A*), as shown in Figure 1, is the first prototype model without the improvements subsequently realized and evaluated in the *RB11.1_B* model (henceforth named *B*), in order to reduce the drag and increase the down-forces. The enhancements applied in the model *B* consist in the implementation of a *front wing*, in removing the *excess surface of the headrest,* in the introduction of *rear extractors* and in the introduction of the *rear hood*. The couples of figures (a) and (b) from 11 to 18, highlight the improvements, described below, achieved with the previous changes. The series of figures (a) concern model *A* while series (*b*) shows results obtained from model *B*. Figures 11 show the polyhedral mesh of the two models. To contain the computational time, these meshes are defined coarser than that of the previous nose's model. If carried out for comparative analysis, as is in the present case, this choice does not affect the quality of results. The meshes are characterized by approximately 4 million volumetric cells, a boundary layer with a thickness equal to 4.9mm, subdivided with 4 sub-layers distributed starting from the shell, with a geometric progression with a *common ratio* 1.5 and a consequent wall-layer equal to 0.6mm.

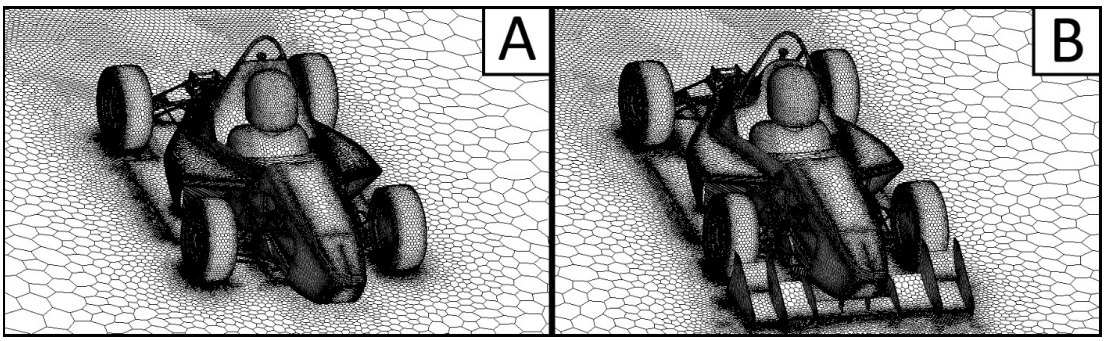

Fig. 11. Polyhedral volume meshes: model A, model B.

5.2. Results and comparative analysis

The first improvement, obtained removing the excess *surface* of the headrest, is labeled with *X* in Figure 12 (a). This change, obviously, directly influences the drag coefficient, interacting perpendicularly with the air flow. The ground effect generated by the front wing is well evident in Figure 13; it is shown in terms of total pressure exerted on the shell surface, whose growing produces a correspondent increase of the down-force. increasing the stability of the car, especially in the parts less fast of the circuits. A further attribute that enhances the ground effect is constituted by the rear air extractors, whose effect is shown in Figure 14; they concur to the generation of the desired '*Venturi*' geometry with a positive effect on the down-force, due to a reduction in total pressure in case *B* compared to *A*. Figure 15 shows another beneficial effect coming from the adoption of the front wing whose cross sections are visible in a transparent way. As a matter of fact, the wings that divert the flow of air towards the top of the shell, increase the down-force on the vehicle. In addition, it is also clear an appreciable reduction in drag due to the shield carried by the wings on the front wheels.

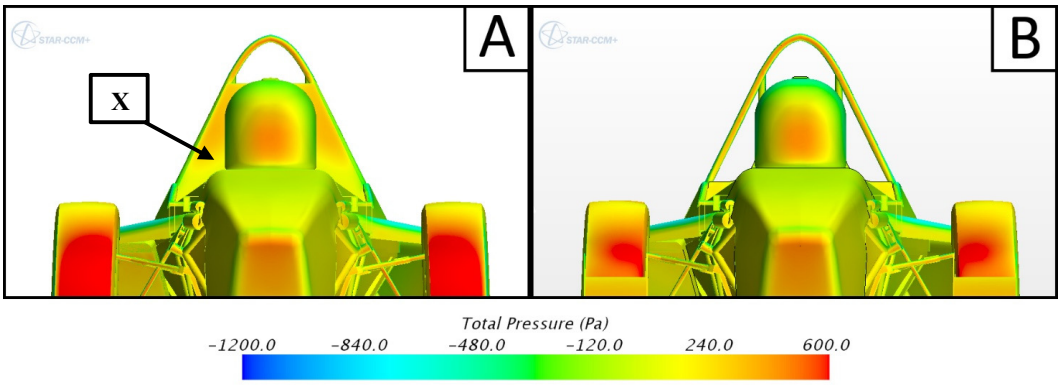

Fig. 12. Headrest modification.

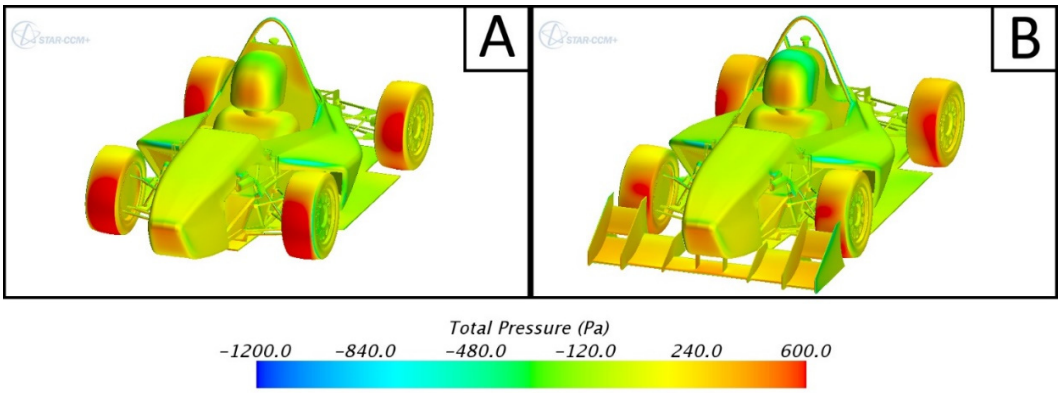

Fig. 13. Effect of the adoption of the front wing.

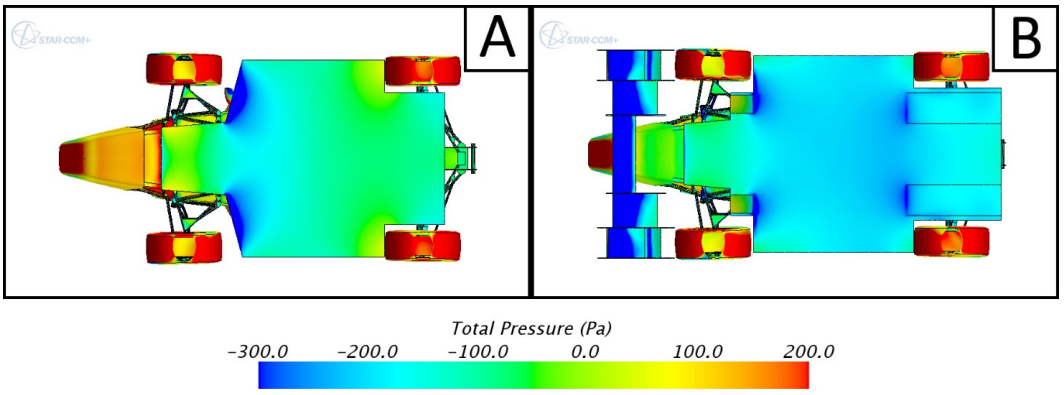

Fig. 14. Effect of the adoption of the extractor.

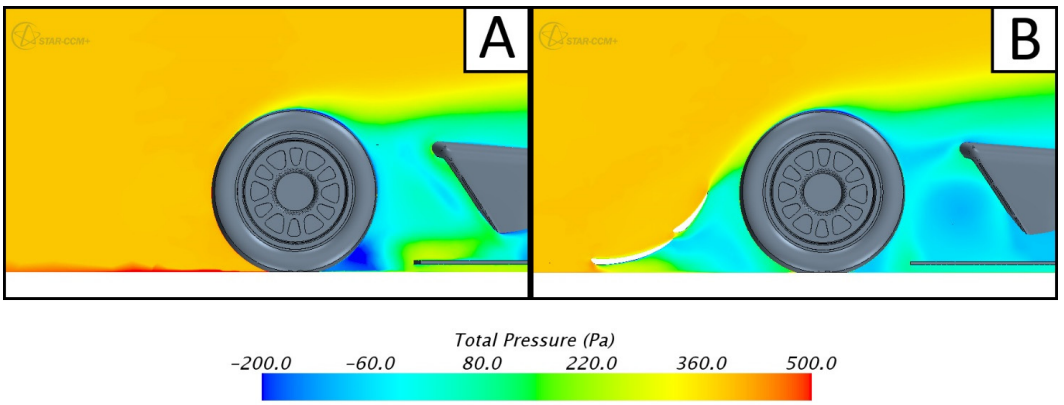

Fig. 15. Effect of the front wing on the front wheel.

The stream lines technique is another way to appreciate the benefits obtained with the changes made to the original model *A*. Stream lines allow to appreciate the quality of the flux; Figures 16 and 17 show, respectively, the effects of the *rear hood* and of the *underbody*, while Figure 18 offers an overall view of the improvements obtained with the model *B*. A more regular flux is a clear evidence; in some areas it is evident the disappearance of recirculation and stagnation points.

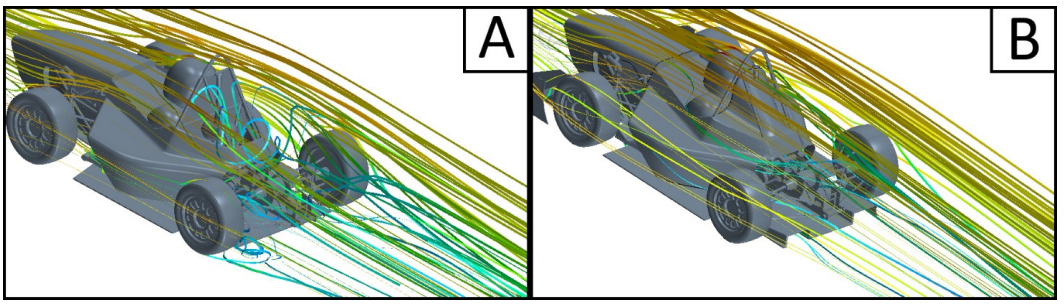

Fig. 16. Stream lines before and after the adoption of the rear hood.

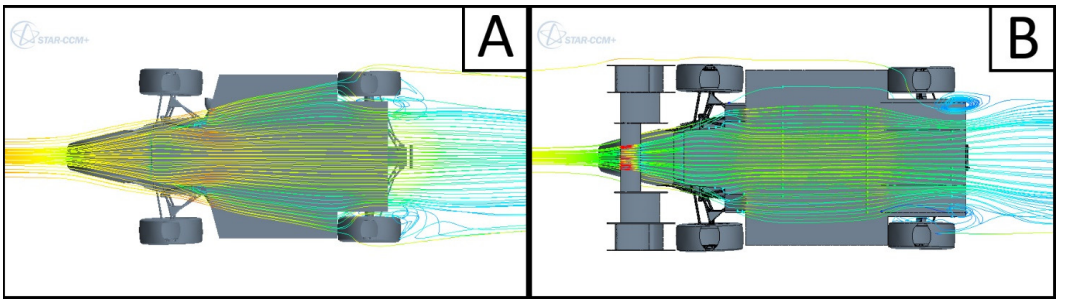

Fig. 17. Stream lines before and after the adoption of the extractor.

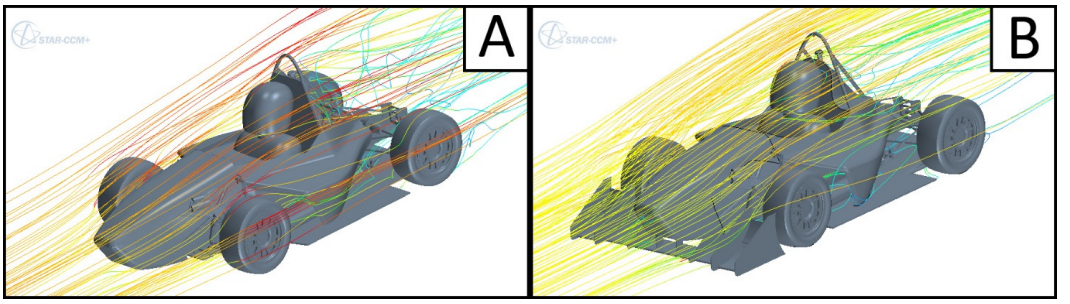

Fig. 18. Stream lines before and after the adoption of the front wing.

5.3. Analysis of the aerodynamic forces and weight distribution

It follows some quantitative analysis based on the comparison between model *A* and *B;* in particular the evaluations were made both on the entire car - where the values, in terms of total drag, are equal to 352 N (model A) and 301 N (model B) - and on some significant components in terms of down-force and drag.

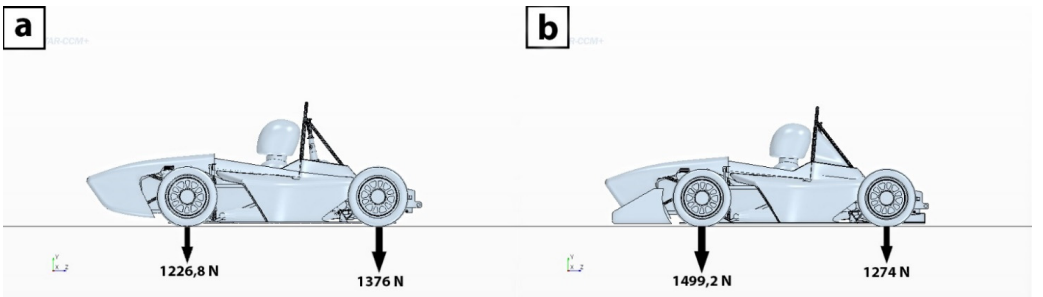

Fig. 19. down-forces evaluation on the original (a) and on the modified (b) vehicle.

Figure 19 shows the sketches of profiles *A* and *B* with the *down-forces* acting on the front and rear wheels. Figure 20 is an alternative and more accurate way of interpreting these results; in fact, for each component of model *B,* not present in *A,* and for the components of *A* modified in *B,* it has been evaluated a quantity named *improvement*, defined as follows:

$$I = \frac{F_B^i - F_A^i}{\left|F_A^i\right|} \cdot 100 \tag{4}$$

Where F_A^i and F_B^i represent the value of the forces acting on the component i^{th} of model A and B respectively; accordingly, positive values express an increase while the negatives a decrease of the force acting on model B compared to A. Generally, there is a remarkable improvement in all the components. Incidentally, as easy to understand, it is noted that the increase of the drag force in the nose is due to the introduction of the front wing; in fact, in model B, the *nose* label means the set consisting of the original nose and front wing.

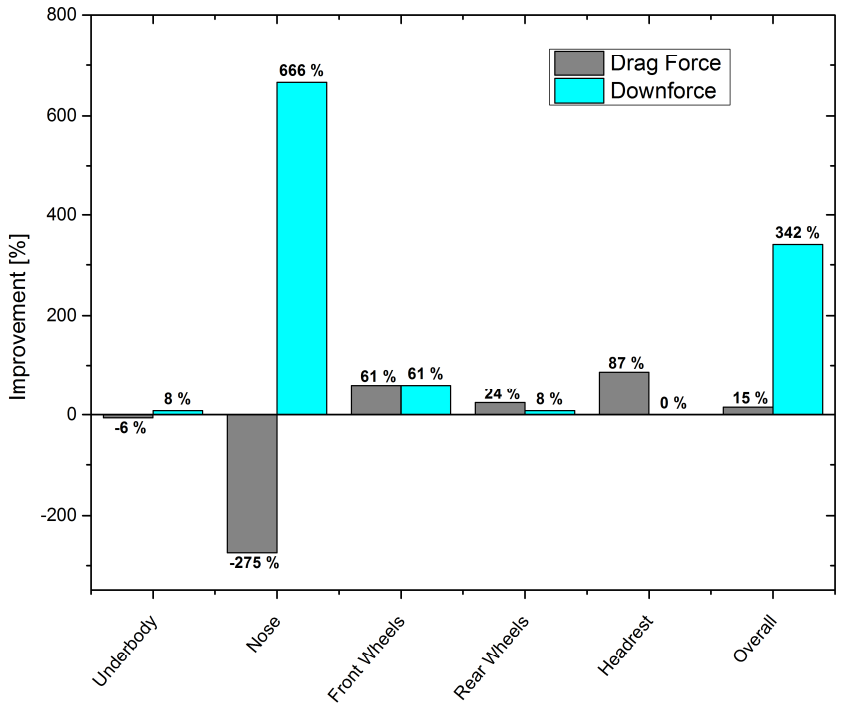

Fig. 20. Percent improvement of the forces on the model B in relation to the model A.

6. Conclusions and future activities

In the present work, an experimental and numerical analysis of the Formula-SAE race car of the University of Perugia, has been presented. In the second part of the work, the numerical comparative analysis, between model A and B, has shown an interesting global enhancement, evidencing the contribution that each new component and each change has brought in terms of down-force and drag.

With regard to future activities, in view of the participation to the next 2014 Formula-SAE meeting - that will be held in Spain - the technical team will be involved in the development of various improvement activities. Concerning the external aerodynamics activities, the main task will be the experimental and numerical evaluation of the forces acting on the full car in model B setting. In particular, for the numerical modeling activity, it will be important to investigate the optimization of the number of the sub-layers; in fact, in the present work the oversizing of the number of the layers defined near to the shell's skin is evident.

References

[1] Dean E. Case "*Formula SAE - Competition History 1981 - 1996*", SAE Technical Paper 962509, 1996, doi:10.4271/962509.

[2] SAE, *2005 Formula SAE Rules, US Comp Edition*, Society of Automotive Engineers, USA, 2004.

[3] Wordley, S., and Saunders, J., "*Aerodynamics for Formula SAE: Initial design and performance prediction*", SAE Technical Papers (2006).

[4] Wordley, S., and Saunders, J., "*Aerodynamics for formula sae: a numerical, wind tunnel and on-track study*", SAE Technical Papers (2006).

[5] Chen, M.N., et al. "*Computer-Aided Front and Rear Wings Aerodynamic Design of a Formula SAE Racing Car*", Applied Mechanics and Materials 120 (2012): 20-25.

[6] Jawad, B.A., Longnecker M.M., Nagy, K., Timmer J.S., "*Aerodynamic Drag and Fuel Economy in a Formula SAE Racing Style Vehicle*", SAE Technical Paper 2001-01-2554, 2011.

[7] Bagal V., Mulemane, A., "*Aerodynamic Drag Simulation and Validation of a Crossover*", SAE Technical Paper 2010-01-0757, 2010.

[8] Huminic, A., Huminic G., "*CFD Study Concerning the Influence of the Underbody Components on Total Drag for a SUV*", SAE Technical Paper 2009-01-1157, 2009.

[9] Friedl, C., Watts, M., "*Drag Coefficient Measurement, CFD Simulation and Validation of an Automotive Body*", SAE Technical Paper 2013-01-1363, 2013.

[10] Roy, S., Srinivasan, P, "*External Flow Analysis of a Truck for Drag Reduction*", SAE Technical Paper 2000-01-3500, 2000.

[11] Mckay, N.J., Gopalarathnam, A., "*The Effects of Wing Aerodynamics on Race Vehicle Performance*", SAE Technical Paper 2002-01-3294, 2002.

[12] Doddegowda, P., Bychkovsky, A.L., George, A.R., "*Use of Computational Fluid Dynamics for the Design of Formula SAE Race Car Aerodynamics*", SAE Technical Paper 2006-01-0807, 2006.

[13] Scappaticci, L., Risitano, G., Battistoni, M., and Grimaldi, C., *"Drag Optimization of a Sport Motorbike"*, SAE Technical Paper 2012-01-1171, 2012, doi:10.4271/2012-01-1171;

[14] S. Watkins, J.W. Saunders, P.H. Hoffmann, *"Comparison of road and wind-tunnel drag reductions for commercial vehicles"*, Journal of Wind Engineering and Industrial Aerodynamics, Volume 49, Issues 1–3, December 1993, Pages 411-420, ISSN 0167-6105.

[15] M. Gohlke, J.F. Beaudoin, M. Amielh, F. Anselmet, *"Shape influence on mean forces applied on a ground vehicle under steady cross-wind"*, Journal of Wind Engineering and Industrial Aerodynamics, Volume 98, Issues 8–9, August–September 2010, Pages 386-391, ISSN 0167-6105.

[16] Mahmoud Khaled, Hicham El Hage, Fabien Harambat, Hassan Peerhossaini, *"Some innovative concepts for car drag reduction: A parametric analysis of aerodynamic forces on a simplified body",* Journal of Wind Engineering and Industrial Aerodynamics, Volumes 107–108, August–September 2012, Pages 36-47, ISSN 0167-6105;

[17] Mathieu Roumeas, Patrick Gillieron and Azeddine Kourta, *"Drag reduction by flow separation control on a car after body"*, International Journal for Numerical Methods in Fluids, Volume 60, Issue 11, pages 1222–1240, 20 August 2009, DOI: 10.1002/fld.1930.

[18] Cheng, S.Y., Tsubokura, M., Nakashima, T., Nouzawa, T., Okada, Y., "*A numerical analysis of transient flow past road vehicles subjected to pitching oscillation"*, Journal of Wind Engineering and Industrial Aerodynamics, Volume 99, April 2011, Pages 511-522.

[19] F. Muyl, L. Dumas, V. Herbert, *"Hybrid method for aerodynamic shape optimization in automotive industry",* Computers & Fluids, Volume 33, Issues 5–6, June–July 2004, Pages 849-858, ISSN 0045-7930.

[20] C. Regert, T. Lajos, "*Description of flow field in the wheelhouses of cars"*, International Journal of Heat and Fluid Flow, Volume 28, Issue 4, August 2007, Pages 616-629, ISSN 0142-727X, http://dx.doi.org/10.1016/j.ijheatfluidflow.2007.04.017.

[21] B. Khalighi, S. Jindal, G. Iaccarino, "*Aerodynamic flow around a sport utility vehicle - Computational and experimental investigation*", Journal of Wind Engineering and Industrial Aerodynamics, Volumes 107–108, August–September 2012, Pages 140-148.

[22] Guilmineau, E., "*Computational study of flow around a simplified car body*", Journal of Wind Engineering and Industrial Aerodynamics, Volume 96, August 2007, Pages 1207-1217.

[23] Scappaticci, L., Risitano, G., Battistoni, M., Desideri, U., Grimaldi, C.N., "*On the influence of the vehicle speed on the aerodynamic drag of road motorcycles*", Third International Conference on Applied Energy - 16-18 May 2011 - Perugia, Italy.

[24] Menter, F. R. (1993), "*Zonal Two Equation k-ω Turbulence Models for Aerodynamic Flows*", AIAA Paper 93-2906.

[25] Menter, F. R. (1994), "*Two-Equation Eddy-Viscosity Turbulence Models for Engineering Applications*", AIAA Journal, vol. 32, no 8. pp. 1598-1605.

[26] Menter F.R., Kuntz M., and Langtry, R., "*Ten Years of Industrial Experience with the SST Turbulence Model*", Turbulence, Heat and Mass Transfer 4,Hanjalić, K., Nagano, Y., and Tummers, M., (Editors), ©2013 Begell House, Inc.

[27] Ramakrishnan, V., Soundararaju, D., Karbon, K., and Jha, P., "*A Numerical Approach to Evaluate the Aerodynamic Performance of Vehicle Exterior Surfaces*," SAE Technical Paper 2011-01-0180, 2011, doi:10.4271/2011-01-0180.
[28] Golovanevskiy, V.A., Chmovzh, V.V., Girka, Y.V., "*On the optimal model configuration for aerodynamic modelling of open cargo railway train*", Journal of Wind Engineering and Industrial Aerodynamics, Volumes 107–108, August–September 2012, Pages 131-139.